Versatile use of droplet coagulation : shaping fine-grained SiO_2 and Al_2O_3 waste streams into monodisperse microspheres

Reference:

Pype Judith, Michielsen B., Mullens S., Meynen Vera.- Versatile use of droplet coagulation : shaping fine-grained SiO_2 and Al_2O_3 waste streams into monodisperse microspheres

Sustainable Materials and Technologies - ISSN 22149937 - 14(2017), p. 19-28

Full text (Publisher's DOI): http://dx.doi.org/doi:10.1016/J.SUSMAT.2017.11.001

Versatile use of droplet coagulation: shaping fine-grained SiO_2 and Al_2O_3 waste streams into monodisperse microspheres

J. Pype[a,b*], B. Michielsen[a], S. Mullens[a], V. Meynen[b]

[a] Sustainable Materials Management, Flemish Institute for Technological Research NV – VITO NV, Boeretang 200, 2400 Mol, Belgium
[b] Laboratory of Adsorption and Catalysis (LADCA), Department of Chemistry, University of Antwerp, CDE, Universiteitsplein 1, 2610 Wilrijk, Belgium

* Corresponding author: bart.michielsen@vito.be

Abstract

The versatile use of droplet coagulation to recycle complex waste resources (fly ash FA, rice husk ash RHA and alum sludge AS) was investigated. Monodisperse microspheres were shaped, creating higher impact on the applicability of the waste resources. In order to obtain a suspension with appropriate rheological properties, pre-processing was required for the AS powder in contrast to the RHA and FA powders. Furthermore, the impact of the shaping process and waste stream properties on the calcination and sintering was determined and correlated to the microstructure of the sintered spheres. The porosity of the sintered AS microspheres was significantly lower (4%) as compared to the FA (50%) and RHA (67%) microspheres. Consequently, the crushing strength of the sintered microspheres varied for the different waste resources. Due to the enhanced densification, the highest crushing strength (185 MPa) was obtained for the AS microspheres.

Keywords

Droplet coagulation, shaping waste powders, rice husk ash, fly ash, alum sludge

Highlights

- Microsphere properties are affected by waste origin, composition and morphology
- Pre-processing of AS is required to obtain a suitable rheology for the droplet coagulation suspension
- Influence of the coagulation precursor (Ca^{2+}) on thermal processing of waste resources

1. Introduction

There is a growing awareness that current material consumption is not sustainable. This requires the prevention of loss of materials out of the material cycles in an economical way. By reusing waste streams as valuable raw materials in industrial applications, it is possible to close the material loop[1][2]. Thereby, it is preferred to add extra functionalities, allowing it to be used in added-value applications[3][4] while limiting the hazardous issues of handling fine-grained waste streams[5]. The fine-grained waste streams often contain crystalline silica that could cause silicosis, certainly when their dimensions are small. A colloidal method such as droplet coagulation is used as shaping method, to limit dust formation and create higher impact on the applicability of these resources. Fine-grained inorganic powders are an important category of solid waste streams varying in origin, chemical composition and morphology. These waste streams are often mixtures of different oxides (silica, alumina, iron oxide, calcium oxide, etc.) and the degree of impurities varies according to the origin of the waste stream[6][7][8]. The aim of this research is to study the generic use of droplet coagulation on waste resources with variety in origin, composition and morphology.

One of the key industrial activities that produce these kinds of solid waste streams are combustion processes. The worldwide coal firing for power generation causes an annual production of 750 million tons of fly ash[9]. Since the chemical composition of the fly ash is determined by the type of coal, a wide variety of compositions is described in literature. However, it could be noted that the principle components are silica, alumina, iron oxide and calcium oxide[9]. The depletion of fossil fuels for the generation of power supply has stimulated the utilization of biomass as a source of fuel, creating a different type of combustion based waste streams. Among the various biomass resources, rice husk is one of the key residues for the energy production[10]. The combustion of the rice hulls, in order to acquire energy, leads to the production of rice husk ash consisting of high amounts of silica[7]. Another type of fine-grained waste powders is generated by a very different type of process: waste water treatment. One of the typical sludges produced is alum sludge, which originates from the addition of an aluminium salt (e.g. $Al_2(SO_4)_3$) to the polluted water. The Al^{3+} ions enable the coagulation of natural organic matter (NOM) in the sludge. In the subsequent processes (flocculation, sedimentation and centrifugation), the NOM is collected in the sludge together with the ions of the aluminium salt[11]. Typically, the alum sludge consists of a high amount of alumina polymorphs and organic material in combination with minor amounts of silica and other impurities. There is still little information

on global alum sludge production, however the large sludge volumes and environmental drawbacks (discharge of aluminium in residuals causing a threat to aquatic life [12]) are an incentive to investigate the valorisation of this waste product[8]. Current research stipulates the valorisation of these waste streams by making use of gel casting such as the here described droplet coagulation.

Gel casting is typically achieved by the polymerization of specific monomers, using binders which are present in the casting suspension (e.g. acrylamides) [13][14]. One of the disadvantages of this method is the emission of toxic volatiles during thermal post processing. A suitable alternative to overcome this aspect is the use of bio-binders, such as sodium alginate[15][16][17]. Sodium alginate is a natural polysaccharide composed of two monomeric units: 1,4-linked β-d-mannuronic (M) and α-l-guluronic (G) acid residues. The solidification of the sodium alginate is achieved by the ionotropic gelation of the guluronic acid residues with a non-monovalent ion (e.g. Ca^{2+}). These non-monovalent ions, inherent to the coagulation mechanism, are incorporated in the microspheres and have a distinct effect on the thermal post processing of the microspheres[18]. However, the impact of the coagulated Ca^{2+} has been elucidated on pure alumina, other influences might be expected when using different waste fines. Here we show how the unique composition of the waste fines interacts with the coagulated calcium upon sintering. Shaping microspheres by use of the droplet coagulation technique is based on an extrusion dripping principle[19]. In this method, a ceramic suspension containing sodium alginate binder is extruded through a nozzle at low volumetric rates. The detachment of the droplet is driven by the gravitational forces on the droplet[20]. The droplets are collected in a coagulation bath containing calcium ions as solidification agent. So far, droplet coagulation has only been demonstrated on pure ceramic suspensions and not on powder resources with variation in composition and origin[21]. The wide variation in composition might cause some difficulties by interaction with the sodium alginate of the gel casting suspension. One of the key requirements for being able to shape an inorganic powder into microspheres by droplet coagulation is the ability to prepare a stable suspension. If not possible, pre-processing of the powder would be required prior to the suspension preparation[22]. The necessity of pre-processing waste powders for droplet coagulation has not yet been elucidated.

The complexity of waste powders (e.g. inhomogeneity of the components, leaching behavior, presence of specific impurities) could cause difficulties in the shaping process. Our aim is to reveal the impact of the varying chemical composition and morphology of waste powders on the different aspects of the shaping process. Therefore, three different

inorganic waste powders were selected to investigate the generic approach and flexibility of the droplet coagulation technique to produce microspheres from recovered waste.

Changes originating from the differences in chemical and physical properties of the powders can be expected in different parts of the microsphere formation: during suspension preparation, the coagulation process as well as the thermal post processing. Studying the impact of the waste type, its origin (e.g. sludge or powdered from combustion processes), composition (e.g. Si/Al ratio) and morphology, on these different aspects is the focus of this work. Vice versa, the impact of the shaping process on the final materials properties is revealed.

2. Materials and methods

2.1. Materials

Alum sludge (AS) was collected at the water production center (Kluizen, Belgium). The sludge is generated by a coagulation-flocculation process to purify the waste waters, requiring the addition of $AlCl_3$ as coagulant, flocculant (Superfloc 100-N, non-ionic polyacrylamide) addition[23] and pH adjustment (H_2SO_4). The AS was dried 24 hours at 100 °C prior to characterization of the powder and listed as AS-D. Siliceous coal combustion fly ash (FA) from the Tarong Power Station (Australia) was used as fly ash source. Silpozz (NK Enterprises, India) was used as the source of rice husk ash (RHA). Characteristics of the waste materials are described in section 3.1. Sodium alginate Br-W was supplied by Brace GmBH (Alzenau, Germany). Furthermore, calcium chloride (Sigma Aldrich, anhydrous, powder ≥ 97 % pure), isopropyl alcohol (98%) and RO water (< 5 µS/cm) were used in this work.

2.2. Shaping microspheres by droplet coagulation

Dried AS-D was calcined (1h) at 600 °C (heating rate 2°C/min) under ambient air and pressure to obtain calcined alum sludge granules. Afterwards, the calcined granules were ball milled at 400 rpm for 30 minutes using tungsten carbide grinding balls of 30 mm (20 wt% powder per milling jar) in order to obtain the calcined alum sludge powder (AS-C). AS-C was washed with milli-Q water in a ratio of 1:10, by shaking it 5 minutes prior to centrifugation at 4000 rpm. The pure milli-Q water contained 7.8 µg/l Al^{3+} and 139 µg/l Ca^{2+}. The washing water was decanted before drying the washed alum sludge at 100°C for 24h. The final alum sludge after 2 wash cycles and drying is listed as AS-C-2W. The RHA and FA powders were used as received. For all waste powders, a ceramic suspension

containing 30 wt% of the waste powder was prepared by planetary mixing it with 1 wt% of alginate Br-W and RO water. The suspensions containing RHA or FA were loaded in a syringe connected with a 600 µm nozzle (Nordson EDF). Droplets were generated by manual pressure on the syringe and collected in the coagulation bath containing $CaCl_2$ and left inside overnight to complete the solidification. Instead of using manual pressure on the syringe, alum sludge droplets were generated by air pressure. As indicated in literature[24], little effect is visible on the size and shape of the spheres when applying different pressures. Therefore, the produced RHA, FA and AS microspheres (RHA-MS, FA-MS, AS-MS) are comparable in this work. After completing the solidification, the microspheres were thoroughly washed with tap water followed by RO water to remove the excess of calcium ions. As a last step in the washing procedure, the microspheres were washed with isopropyl alcohol to reduce the capillary pressure during drying. Subsequently, the samples were dried at 105°C for 24 hours and sintered 1 hour at varying temperatures with a heating rate of 2 °C/min under ambient air and pressure conditions.

2.3. Characterization techniques

The chemical composition of the starting powders was determined by a high performance energy dispersive XRF (X-ray fluorescence) spectrometer with polarized X-ray excitation geometry (HE XEPOS, Spectro Analytical Systems, Kleve, Germany). The instrument was equipped with a 50 W tungsten end window tube (max. 60 kV, 2 mA) and a Silicon Drift Detector. All analyses were performed under He atmosphere. The samples were ashed at 1000 °C during 4 hours in a muffle furnace (Thermolyne, Iowa, USA). About 0.9 g of the ashed sample was subsequently mixed in a platinum crucible with a 100% lithiumtetraborate flux (XRF Scientific, Brussels, Belgium) in a flux:sample ratio of 10:1. The fusion was performed with an automatic fusion system (XrFuse 2, XRF Scientific, Brussels, Belgium), in which the sample was fused at 1250°C during 11 minutes. An ammonium iodide tablet (XRF Scientific, Brussels, Belgium) was added as release agent. The fused sample was removed from the furnace and poured into a pre-heated mold. During cooling, fan-forced air was applied to accelerate the solidification of the beads. For the XRF measurement, the fused bead sample was placed in the auto sampler of the EDXRF system.

Furthermore, the raw waste powders were examined using a cold field emission scanning electron microscope (FEGSEM) of the type Nova Nano SEM 450 (FEI, USA) at 5 kV. In addition, sintered microspheres were measured using the FEGSEM at 20 kV. Before the measurement, the microspheres were encapsulated in epoxy resin and cured at room temperature. Subsequently, the samples were cut and polished in order to analyze the

cross-section of the microspheres. Element mappings of the raw RHA and FA powders, pre-processed AS-C and cross-sections of the sintered microspheres were performed with a Bruker XFlash Detector 5030 and a Bruker QUANTAX-200 EDS system.

The cation concentration in the wash water was determined by inductively coupled plasma atomic emission spectroscopy (ICP-AES) on a 5100 ICP-AES of Agilent. Sulfate concentrations were determined by ion chromatography (IC) on a Metrohm 850 Professional IC, connected with a Professional UV/VIS detector.

Rheology of the suspensions was analyzed with a Haake Mars Rheometer using a concentric cup measuring geometry (cup Z43 DIN 53018 and rotor Z41 DIN 53018). The dynamic viscosity was recorded in function of the shear rate (0.01 – 1000 s^{-1}) and data points were collected when decreasing the shear rate. The rheology analysis was performed at a controlled temperature of 25 °C.

The shaped microspheres were analyzed by optical microscopy using a Zeiss Discovery V12 stereomicroscope, equipped with a Plan Apo S 1.0 w FWD 60 mm objective. Images of the microspheres were taken by an Axiovision MRc digital camera connected to the optical microscope. Image processing was performed by Axiovision Rel. 4.8 software using the same procedure as explained in earlier work [18]. Image analysis was performed on at least 20 microspheres. The average microsphere size is reported with its standard deviation.

Thermogravimetric analysis (TGA) was recorded on a STA 449 F3 Jupiter (Netzsch, Germany) under a flow of dry air (50 ml/min). The samples were analysed from ambient temperature to 1500 °C with a heating rate of 10 °C/min. The TGA apparatus was coupled online with a quadrupole mass spectrometer TGA/STA-QMS 403 D Aëolos (Netzsch, Germany) by a heated capillary (200 °C)

The dilatometry analyses were performed on a DIL 402 C dilatometer (Netzsch, Germany) in dry air (70 ml/min). Pellets were pressed from the waste powders and crushed microspheres. The FA and RHA raw powders required the addition of 1 wt% alginate Br-W to enable pressing. Dilatometry analysis (10°C/min) on the RHA and FA (powder and microspheres) pellets was limited to 1350 °C due to the melting of the sample. The dilatometry analysis on the AS pellets was performed up to 1600 °C.

In addition, the crystal phases of the microspheres were analysed by X-ray diffraction (XRD) analysis. The sintered microspheres were ball milled before performing the analysis. The diffraction spectra were collected on a PANalytical X'Pert Pro MPD diffractometer with filtered Cu Kα radiation. The analysis was performed in the 2Θ mode using a bracket sample holder with scanning speed of 0.04°/4s continuous mode. Phase identification was

made by searching the ICDD (International Centre for Diffraction Data) database for inorganic compounds.

The crushing strength of the microspheres was assessed by side crushing strength (SCS) testing using an Instron 5582 Universal testing machine. Couroyer et al. [25] calculated the side crushing strength σ_f using the following equation:

$$\sigma_f = 2.8 \frac{P_f}{\pi D^2}$$

P_f is the load (N) at the breaking point of the microspheres and D the diameter (m). The strength of a single microsphere is collected between two diametrically opposed contact points. At least 10 spheres are crushed to calculate the average strength of a single shaped microsphere. The standard deviation of the results was calculated and reported along the average crushing strength.

3. Results and discussion

3.1. Waste powder characteristics and pre-processing requirements

Shaping microspheres of the fine-grained waste powders using droplet generation requires a stable suspension. One of the main differences between the waste powders applied in this study is the presence of organic additives such as the flocculant in the alum sludge. This flocculant is added to waste water to induce agglomeration of microflocs, leading to larger and denser flocs. However, the presence of these flocs in the alum sludge hampers the preparation of a stable suspension with high solid loading for droplet coagulation. Therefore, the flocculant has to be removed by thermal treatment. In order to interpret the thermal decomposition of AS-D and the other materials, calcination profiles were determines. Thermogravimetric analysis coupled with a mass spectrometer (TGA-MS) was used to acquire TG/DTG profiles and mass spectra as shown in Figure 1 and Figure 2. Besides a difference in calcination profile, distinct differences in loss on ignition (LOI) can be noticed between the waste powders originating from high temperatures processes (FA and RHA) and the humid waste powder (AS-D). After heating at 1000 °C (completion of calcination), FA and RHA lost respectively 0.9% and 3.2% of their matter, in contrast to the higher loss of 43.6% of the dried alum sludge.

Small amounts of hydrated water are lost up to 200 °C in RHA and FA, as confirmed by signals of H_2O (m/z = 18) in the MS data. The thermal decomposition of the RHA powder starts at 250 °C with a DTG maximum at 445 °C. The CO_2 (m/z = 44) signal in the MS data can be correlated to the oxidation of residual carbon of the rice hulls[26][27]. The minimal

thermal degradation of the FA powder is characterized by a higher onset temperature compared to the RHA powder. The thermal decomposition starts at 510 °C (DTG maximum: 645 °C), corresponding to the CO_2 signal in the MS data. The weight loss in this temperature range can be correlated to the carbon oxidation of its carbonaceous material after coal combustion, according to the following chemical reaction [28]:

$2C + xO_2 \rightarrow 2CO_x$ (x = 1 or 2)

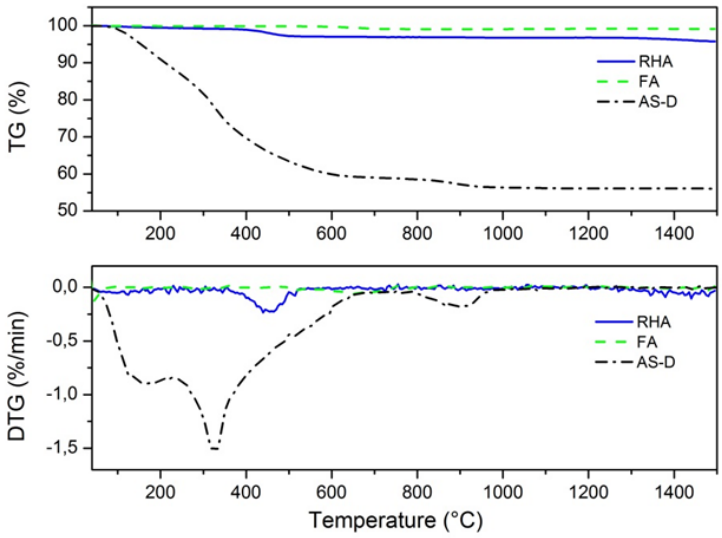

Figure 1: TG and DTG of the waste powders (RHA, FA and AS-D) in function of temperature

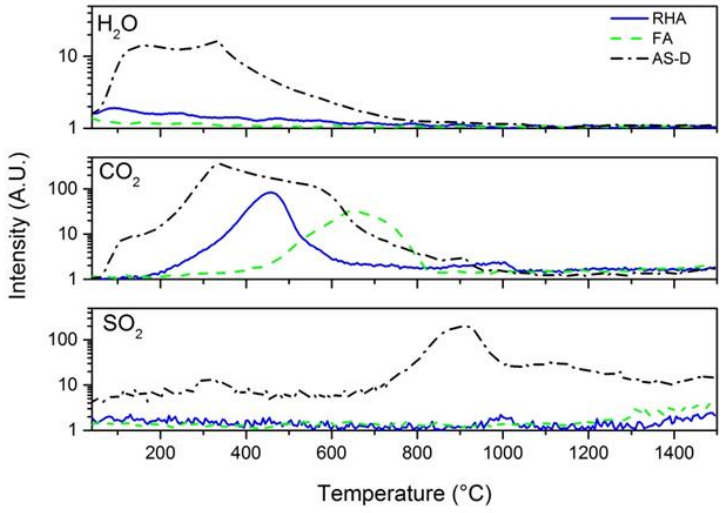

Figure 2: Mass spectra of gaseous components of RHA, FA and AS-D evolving in function of temperature

The calcination profile of the dried AS-D indicates a more complex process with a broad weight loss up to 700 °C. The multiple simultaneously occurring events makes it an

ambiguous identification. However, the main processes can be identified based on the evolution of gaseous components. The MS data in the temperature range from 100 to 800 °C reveals the evolution of H_2O and CO_2. The loss of water can originate from multiple processes such as the phase transformation of the amorphous aluminium hydroxide of the sludge into stable phases by increasing the temperature[29]. Here, H_2O will be formed due to the decomposition of the hydroxide. As indicated earlier in this work, the alum sludge contained natural organic matter (NOM) and flocculant (Figure A1), which also decompose in this temperature range, resulting in the evolution of H_2O and CO_2. The TG analysis of the alum sludge shows another DTG maximum in the temperature range of 800-1000°C, corresponding to the signal of SO_2 (m/z= 64) in the mass spectrum. The presence of sulfur can be explained by the pH buffering step of the waste water treatment, causing the formation of $Al_2(SO_4)_3$ in the alum sludge during thermal processing. The decomposition of this aluminium sulfate occurs at temperature up to 800 °C [30].

$Al_2(SO_4)_3 \rightarrow Al_2O_3 + 3SO_2 + 1.5\ O_2$

TGA-MS analysis on the pure flocculant indicates its complete removal at 600 °C (Figure A1). As pre-treatment, the dried alum sludge was therefore calcined for 1 hour at 600 °C, resulting in large irregular granules. To obtain a size distribution comparable to the ashes (Figure A2), the calcined alum sludge (AS-C) was subsequently ball milled. The resulting calcined and milled alum sludge (AS-C) was further characterized similar to the other two waste powders.

Component		***RHA***	***FA***	***AS-C***
Si	%	43.1	32.7	5.2
Al	%	-	12.7	39.1
K	%	1.0	0.5	-
Ca	%	0.7	-	1.4
Ti	%	-	0.8	-
Mn	%	0.1	-	0.1
Fe	%	0.3	1.4	-

Table 1: Elemental analysis of the waste powders determined by XRF on the melt

Earlier work on droplet coagulation indicated the importance of controlling the composition of the suspension on shaping and sintering microspheres[18][31][32]. The presence of various elements plays a role in the thermal post treatment of the ceramics, inducing the formation of different polymorphs. The elemental composition of the waste powders varies with the origin of the waste process as visible in Table 1 and Figure 3. The two main elements, present in the here applied waste streams, are Si and Al in varying ratios. RHA

contains primarily silicium in its matrix in the presence of minor impurities such as K, Ca, Mn and Fe. Analog to the RHA, FA contains mainly silicium in its matrix, with the prevailing presence of aluminium. One of the common impurities in FA is Fe, as is also indicated in literature[9]. AS-C contains the highest concentration of Al in combination with a minor fraction of Si. Since the here applied alum sludge originates from drinking water treatment, calcium is present as one of the main impurities. SEM-EDX reveals the (in)homogeneity of the various elements in the waste powders in combination with their morphology. Knowledge on the morphology is important as it will have an impact on the powder packing in the microspheres during shaping and drying (Table A1 and Figure A2). The RHA powder consists of irregularly-shaped powder particles since they originate from the processing of fibrous rice hulls. Mapping of the chemical composition revealed a heterogeneous mixture of the impurities in the SiO_2 matrix, indicated by distinct grains of Al_2O_3, CaO and K_2O. The FA powder is a combination of heterogeneous and homogeneous particles. The iron impurities are observed as separate grains in the mixtures, where Al_2O_3 and SiO_2 are merged in the same particles in varying concentration. Additionally, a different morphology was revealed with the clear presence of spherical particles (cenospheres) caused by the combustion process of the coal. In contrast to the waste powders produced in high temperature processes, a homogeneous mixture of elements was visible in the AS-C powder. Ball milling of the calcined granules resulted in a broad size range of irregular shaped grains.

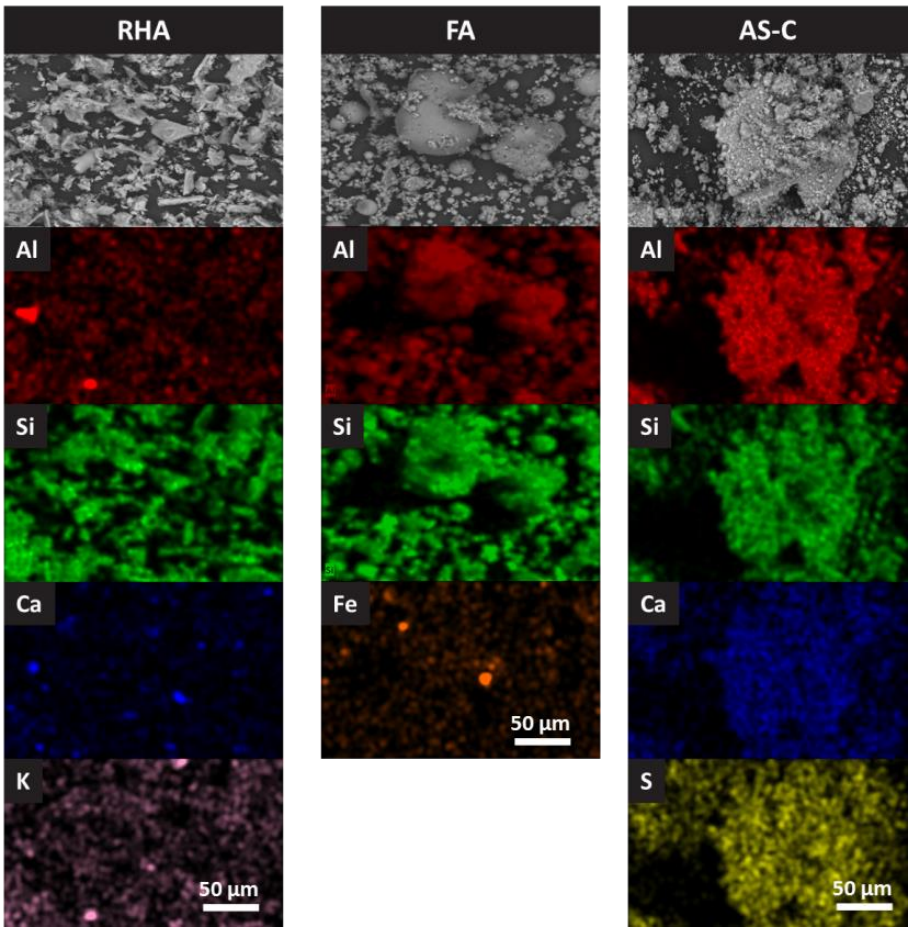

Figure 3: SEM-EDX analysis on the RHA, FA and AS-C powders

The fine-grained waste powders (RHA, FA and AS-C) were added to the sodium alginate solution and water in order to prepare the suspensions. The RHA and FA powders dispersed homogenously in the suspension, in contrast to the AS-C powder. Mixing the AS-C powder in a similar powder loading with sodium alginate resulted in an inhomogeneous rigid structure. Some blocks of coagulated alginate could be distinguished from alum sludge agglomerates. Therefore, only suspensions with very low powder content could be obtained. As indicated in literature, significant amounts of soluble salts are present on the alum sludge even after calcination[22].

As shaping of microspheres is controlled by the ionotropic gelation of sodium alginate in the ceramic suspension induced by the non-monovalent cations in the coagulation bath[33], free cations in the ceramic suspension can interact with the alginate, leading to increased viscosity. To avoid this partial coagulation in the suspension, the AS-C powder was washed with milli-Q water to lower the cation concentration in the powder. The effectiveness of the washing procedure was followed by ICP-AES and ion chromatography to determine the ion concentration (Figure 4).

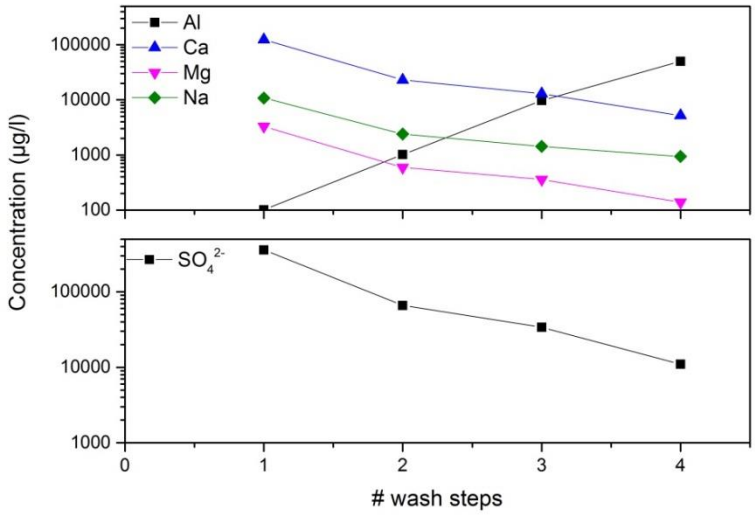

Figure 4: Concentration of cations and sulfate ions in function of the number of wash steps.

An elevated concentration of calcium cations and sulfate ions was determined in the first eluate. Calcium is often reported as the model cation to induce the ionotropic gelation of sodium alginate due to its high efficacy[34]. In the eluate of the following washing steps, the amount of calcium ions decreased substantially. However, an increase in concentration of aluminium ions is observed in function of the wash steps, clearly visible after wash step 3. The amorphous alumina phase tends to leach from the sludge. In addition, a decline in SO_4^{2-} was determined in the wash water. Although no clear impact of the sulfate ions is expected on the suspension, the difference in sulfate concentration will diminish the formation of sulfate phases during the calcination and sintering.

Based on the leaching of calcium cations after the first washing step (124000 µg/l to 23000 µg/l), it was presumed that shaping microspheres with AS-C powder after one wash step (AS-C-1W) would be possible. However, rheological analysis on the suspension revealed shear thinning behaviour indicating that even at these concentrations, there were indications of the presence of a gel network in the suspension (Figure 5). The free movement of the powder particles in the suspension was inhibited due to the gel network, resulting in increased viscosity at low shear rates. In addition, small gel clots were observed in the suspension after standing for 30 minutes. Therefore, the AS-C powder was washed for a second time (AS-C-2W) prior to suspension preparation. In this case, no gel clots could be observed over several hours and the rheological data of the suspension shows similar behaviour to the suspensions prepared using raw RHA and FA powders. All of them are shear thinning at elevated shear rates (above 10 s^{-1}) with indistinct effect as compared with AS-C-1W. This minimal shear thinning behaviour has no effect on the

droplet formation of the suspensions at the nozzle, since this time the gel network can be broken up in definite droplets. [35].

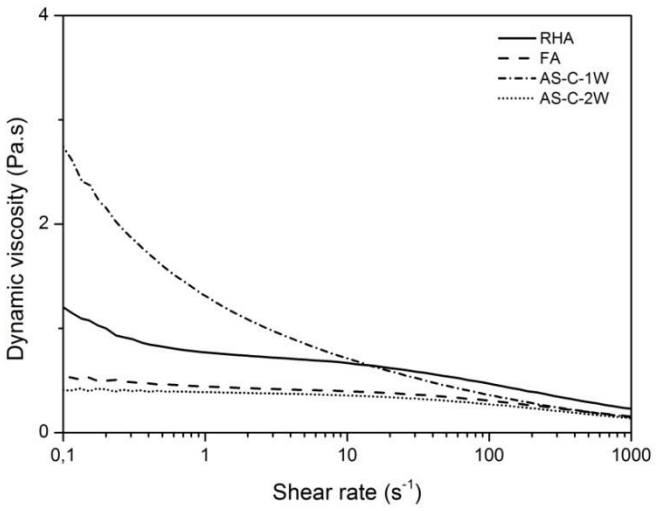

Figure 5: Rheology of the RHA, FA and AS-C suspensions in function of the shear rate. The influence of washing steps on the calcined alum sludge waste powder is denoted as 1W and 2W

3.2. Shaping microspheres

The suspension droplets were collected and solidified in a $CaCl_2$ coagulation bath by the exchange of monovalent sodium ions with divalent calcium ions. The obtained monodisperse microspheres were collected after ageing in the bath for 24 hours followed by rinsing with RO water, isopropyl alcohol and drying. No variation in wet microsphere size of RHA-MS and FA-MS could be observed, despite the differences in viscosity of the suspension (Table 2). In contrast, distinct differences in shrinkage were observed during drying, resulting from differences in powder packing as caused by the variations in powder size and shape (Table 2). The water remaining in the alginate gel network is eliminated by increasing the temperature up to 100 °C, causing a rearrangement of the powder particles in the microspheres. Figure A2 shows the correlation between particle size distribution and feret ratio of the particles. The elongated RHA grains inhibit a compact powder packing during drying, resulting in limited shrinking and thus larger microspheres (2560 ± 69 µm). The FA-MS displayed more shrinkage from wet to dry (19%), due to a higher degree of powder compaction. A twofold effect could be noticed. The FA powder has a broader particle size distribution and higher sphericity level, both increasing the powder compaction in the microsphere. The AS-C powder has an even broader particle size distribution, enhancing the powder compaction even more and causing the highest degree of shrinkage (22%). Dry AS-MS microspheres had the lowest size of 2164 ± 63 µm.

	Av. Diameter Wet (µm)	*Av. Diameter Dry[1](µm)*	*% Shrinkage Wet to dry[1]*	*Av. Diameter Sintered[1] (µm)*	*% Shrinkage Dry to sinter*	*% Porosity[2],**	*Crushing strength (MPa)**
RHA-MS	2893 ± 88	2560 ± 63	12%	2489 ± 63	3%	67%	0.7 ± 0.1
FA-MS	2820 ± 92	2283 ± 95	19%	2217 ± 48	3%	50%	5.3 ± 1
AS-MS	2774 ± 34	2164 ± 63	22%	1384 ± 42	36%	4%	185± 57

Table 2: Overview of microsphere properties. [1] Optical microscopy, [2]SEM analysis on sintered cross section (Sintering: RHA-MS/FA-MS at 1400 °C and AS-MS at 1600 °C)*

3.3. Calcination and sintering

After shaping, a controlled thermal post processing of the microspheres is required to obtain their final properties and strength. The calcination process of the dried microspheres was simulated in the TGA-MS (Figure 6 and 7) and correlated to the analysis on the waste powders (Figure A3, Figure A4 and Figure A5) to be able to distinguish the mass loss induced by the incorporated calcium alginate and the mass losses of the waste powders itself. Analog to the evolution of physisorbed water in the FA and RHA powder, weight losses in the temperature range of 30 – 200 °C were visible. The DTG maxima of the RHA-MS (83 °C) and FA-MS (50°C) are sharp and well defined in contrast to the DTG profile of AS-MS in this temperature range. The weight losses induced by the desorption processes and those of calcination are not resolved in the DTG and thus visible as one broad asymmetric signal. Our previous work on shaping alumina microspheres indicated a two-step oxidation process of the calcium alginate[18], with the intensive evolution of H_2O and CO_2, released by the oxidation of the glycosidic bonds. The first DTG maxima of this process are observed at 280 °C for both the RHA-MS and FA-MS sample. Based on the evolution profiles of H_2O and CO_2, it can be concluded that simultaneously oxidation of the alginate and decomposition of $Al(OH)_3$ occurred within the temperature range of 150 to 600 °C in case of the AS-MS samples. The oxidation of calcium alginate is confirmed by the detection of H_2O and CO_2 (m/z = 44), whereas the $Al(OH)_3$ decomposition only generates H_2O. Concluding from the differences between H_2O and CO_2 signals, the first oxidation step of the calcium alginate appeared analogue in all samples. However, at higher temperatures, differences start to appear. The DTG profile of the RHA microspheres indicates a broad peak between 330 and 600 °C with a maximum at 446 °C. The weight loss in this temperature range is correlated to the oxidation of carboneous material of the RHA powder itself and the second decomposition step of the calcium alginate (decarboxylation). In contrast to the oxidation of the calcium alginate in the RHA-MS sample, an additional peaks can be observed in the FA-MS sample between 330 to 600°C

as compared to the pure FA powder. The First DTG maximum at 380 °C correlates to the further oxidation of alginate fractions corresponding to the H_2O and CO_2 signals. As observed in the CO_2 signal of the MS, the decarboxylation has shifted to higher temperatures with a DTG maximum at 510 °C. The DTG profile of the AS-MS sample revealed additional weight losses above 800°C in contrast to the RHA-MS and FA-MS samples. The decomposition of aluminium sulfate, as determined in the alum sludge powder, occurs between 800 and 1000 °C with its corresponding SO_2 signal in the MS data. However, a slight increase in $Al_2(SO_4)_3$ could be determined (+0.3%) in contrast to the dried alum sludge (AS-D) (Figure 1 and Figure A5). By calcination of AS-D for 1 hour at 600 °C in the pre-treatment, the flocculant structure is decomposed and consequently the flux of released aluminium ions are stabilized by SO_4^{2-} of the sludge. This extra $Al_2(SO_4)_3$ is decomposed in the same temperature range as the initial aluminium sulfate. Alongside the $Al_2(SO_4)_3$ decomposition, CO_2 could be observed in the MS data which could be correlation to the decomposition of $CaCO_3$ of the alum sludge as it is also visible in AS-D. An additional weight loss is detected in the AS-C-2W and AS-MS samples compared to AS-D in the temperature range of 1100 to 1300 °C contributed by the decomposition of calcium sulfate into calcium oxide and sulphur dioxide by the following equation [36][37].

$CaSO_4 \rightarrow CaO + SO_2 + ½\ O_2$

Together with the aluminium stabilisation of the flocculant in the sludge, also calcium was adsorbed on the flocculants surface[38]. Therefore, the calcined flocculant also released calcium in the sludge, resulting in the form of $CaSO_4$ and causing a similar TGA pattern at temperatures above 1000°C as the microspheres (AS-MS). Due to the low solubility of $CaSO_4$, only little amounts are expected to be leached during the washing procedure of the calcined alum sludge[38].

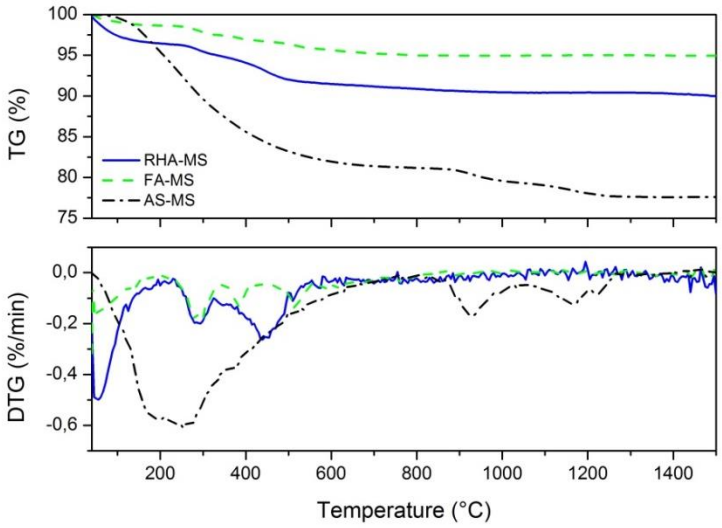

Figure 6: TG and DTG of the dried microspheres (RHA-MS, FA-MS and AS-MS) in function of the temperature

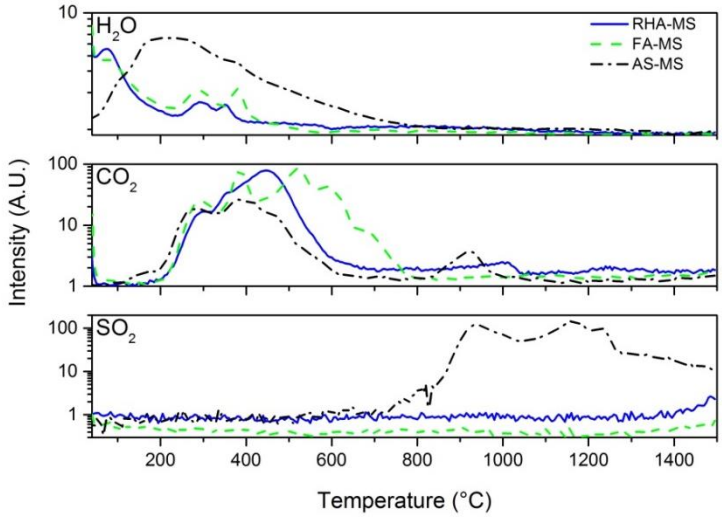

Figure 7: Mass spectra of the gaseous components evolving during TGA of RHA-MS, FA-MS and AS-MS in function of temperature

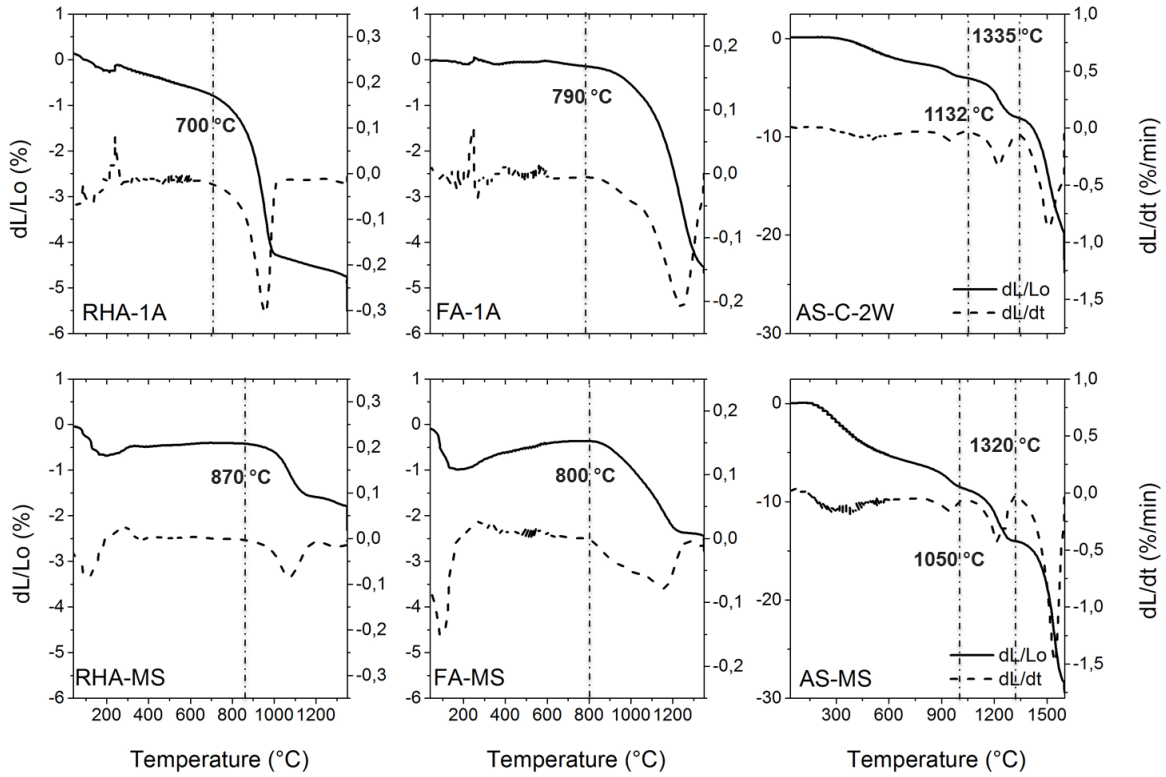

Figure 8: Dilatometry analysis (dL/Lo and dL/dt) on pellets of RHA, FA and AS-C-2W raw powder (1wt% alginate was added as binder in the RHA and FA pellet and therefore listed as RHA-1A and FA-1A) in correlation to pellets of the microspheres (RHA-MS, FA-MS and AS-MS)

The sintering behaviour of the different powders in correlation to their microspheres is shown in Figure 8, with their dilatometry data in Table A2. A distinct difference in sintering behaviour of RHA, FA and AS-C-2W can be noticed, due to their unique chemical composition and morphology. In addition, the dilatometry data shows the impact of the calcium of the sodium alginate coagulation in the sintering of the microspheres compared to the waste powders. In the initial stage, the calcium is present as calcium carbonate, which decomposes at higher temperature into calcium oxide. As visible in Figure 8, the RHA powder (RHA-1A) started to sinter at 700 °C with a total shrinkage of 4.8%. Introducing calcium in the microspheres inhibited the sintering process, shifting the onset temperature to 870 °C and limiting the shrinkage to 1.8%. Sintering of the FA samples started at approximately 800 °C, in correlation with previous work on Tarong fly ash[39]. The presence of calcium had no impact on the onset temperature in contrast to the rice husk ash and alum sludge samples. However, the initial FA-1A sample revealed a higher degree of total shrinkage (-4.6%) compared to the FA-MS microspheres (-2.5%) which followed a more gradual shrinkage between 790 and 1200 °C. Sintering alum sludge

occurs in different steps due to the decomposition of $Al_2(SO_4)_3$ and $CaSO_4$[36]. The first sintering step is observed at 1132 °C for the raw powder (AS-C-2W) in contrast to a lower sinter onset (1050 °C) after shaping into microspheres. However, the maximum sinter temperatures (dL/dt max) are approximately the same for both samples. The difference in onset temperature could be correlated the higher amount of calcium in the microspheres. A sinter plateau was reached at 1250 °C, due to the release of SO_2 gas upon decomposition of $CaSO_4$[36]. The densification process restarted at about 1320 °C, reaching its maximum densification at 1600 °C with the highest level of densification (28.4 %). Due to the differences in sintering behavior of the samples, different variations in sintering temperatures were selected to illustrate the impact on the final microsphere properties. The RHA-MS and FA-MS were sintered between 1200 and 1400 °C. Above 1400 °C, the microspheres began to deform and further examination of the properties was not possible. The AS-MS were sintered between 1400 and 1600 °C, to obtain densification of the microspheres.

3.4. Microsphere properties

In order to identify the impact of sintering on the polymorphs of the microspheres, XRD analyses were performed (Figure 9). The XRD pattern of RHA-MS revealed the presence of two main crystalline components, cristobalite (ICDD card 071-6240) and tridymite (ICDD card 074-8989). It has been reported in literature that the formation of tridymite is promoted by the presence of potassium oxide (K_2O) in rice husk ash [3][40]. Tridymite is the silica crystal phase with the lowest density, enabling the incorporation of interstitial cations, such as K^+, into its open structure. Even though K^+ could be detected via elemental analysis and SEM-EDX of the waste powder and the elemental analysis of the microspheres (Table A3), no potassium could be determined on the SEM-EDX maps of the microspheres (Figure 10). The presence of calcium, however, is clearly visible in both the EDX and as lighter dots in the SEM images of the cross section of sintered RHA-MS. XRF analysis of the microspheres in correlation to their initial powder confirmed the enrichment of calcium in the spheres (Table A3). Nevertheless, no impact of the calcium is visible in the XRD patterns as it gives rise to the formation of an amorphous calcium silicate phase, as known from the phase diagram of CaO and SiO_2[41].

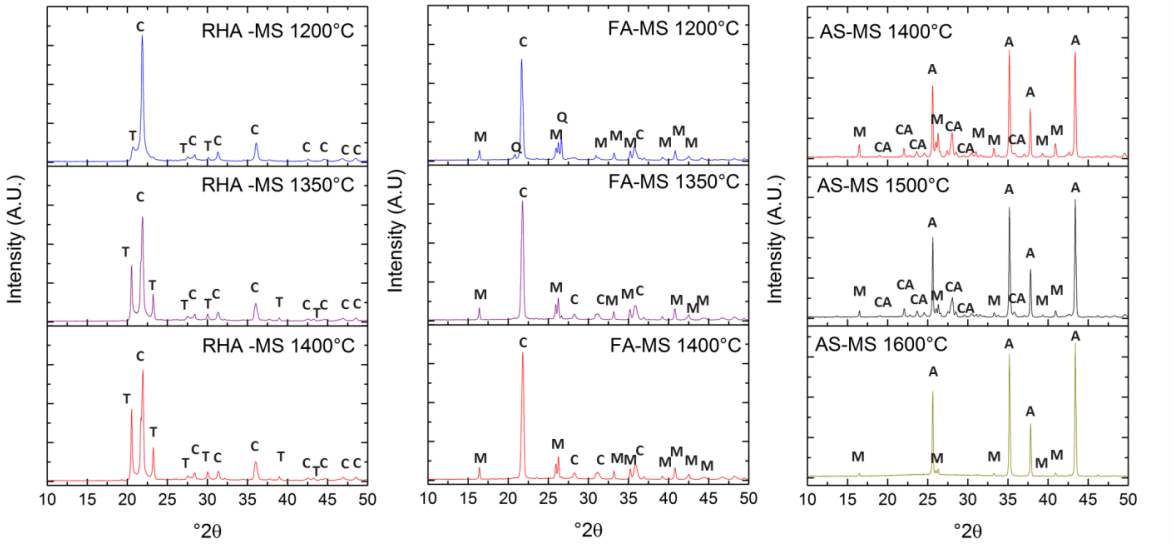

Figure 9: XRD patterns of the microspheres sintered at different temperatures. The different crystal phases are indicated as: α-alumina (A), mullite (M), calcium aluminium silicate (CA), cristobalite (C), quartz (Q) and tridymite (T)

The diffraction peaks of FA-MS after sintering revealed the presence of a mixture of mullite (ICDD card 079-1457) and cristobalite due to the high concentration of alumina and silica in the initial FA powder. The XRD pattern at 1200 °C revealed the presence of quartz (ICDD card 079-1913), which is one of the initial polymorphs of fly ash. Increasing the sinter temperature to 1350 °C eliminated the α-quartz peak simultaneously with the relative increased intensities of cristobalite and mullite[42]. The SEM-EDX confirms the presence of this mullite structure in the SiO_2 matrix via its typically elongated grains [43]. The small amount of iron in the structure (~1.3 % Fe) present as magnetite is expected to transform into hematite based on what has been described in literature[44]. However, due to low intensity of the signal no peaks of magnetite nor hematite were observed. Nevertheless, a much more homogenous spread of iron could be distinguished on the cross section of the sintered microspheres as compared to the Fe distribution in the waste powder (Figure 10 versus Figure 3). The XRD diffractogram of AS-MS shows the presence of α-Al_2O_3 (ICDD card 088-0826) and mullite after sintering at 1600 °C. α-Al_2O_3 is the end product of the thermal conversion of the initial amorphous $Al(OH)_3$ and γ-Al_2O_3 into a stable high temperature polymorph. Additionally, alumina is known to react into mullite in the presence of silica during thermal post treatment[45]. XRD patterns at 1400 °C and 1500 °C show the presence of calcium aluminium silicate (ICDD card 070-0287) in the matrix, induced by the presence of calcium. As described in earlier work, some interaction of calcium with the

alumina phase could be expected[18]. Due to the melting of the calcium aluminium silicate at 1553 °C[46], an amorphous phase was formed in the crystalline structure of alumina and mullite at 1600 °C. Considering this melting behaviour, small amounts of liquid phase were present in between the Al_2O_3 grains enhancing the diffusion along the grain boundaries during sintering. As visible in Figure 10 and Figure A6, several large Al_2O_3 grains can be observed in the mullite and calcium aluminium silicate matrix. SEM-EDX revealed these enlarged grains by the lack of Si and Ca. In addition, the cross-section shows the presence of several of these grains in the microsphere. Consequently, the impurities of the alum sludge enhance the abnormal grain growth (AGG) of Al_2O_3 [47].

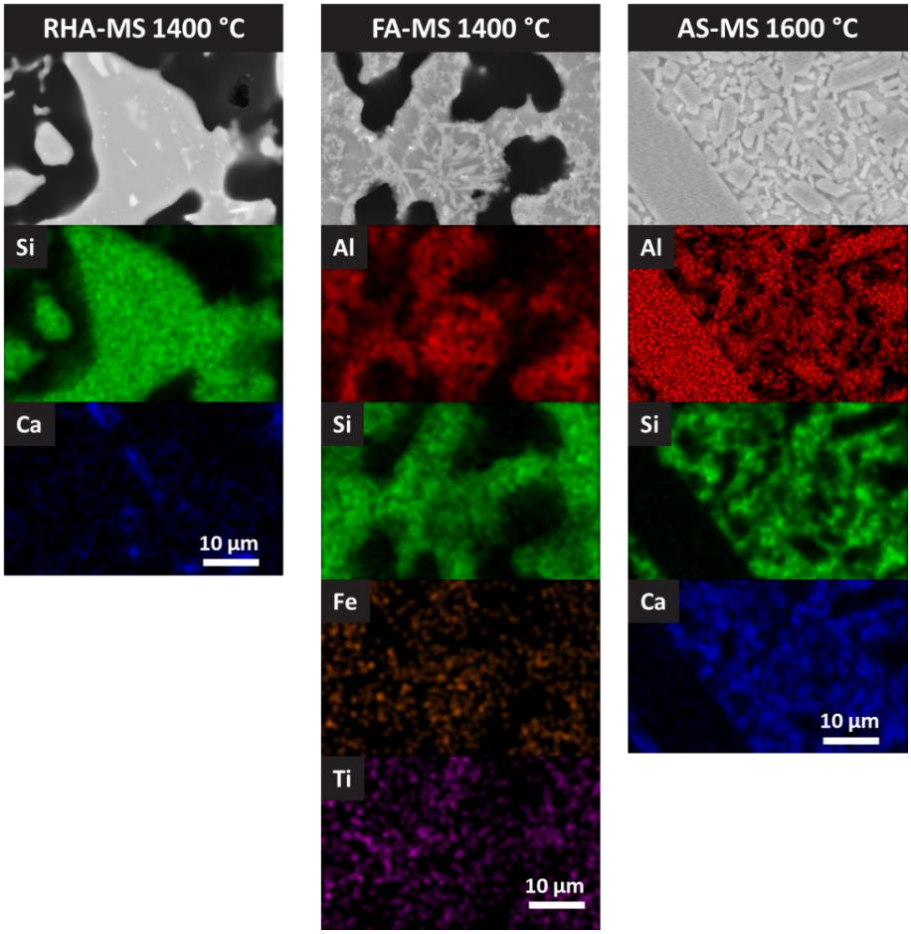

Figure 10: SEM-EDX analysis on the cross section of the microspheres after sintering 1 hour at 1600 °C

Due to the differences in powder morphology and chemical composition, differences in drying and sintering and hence also in residual porosity after sintering could be observed on the SEM images of the cross sections (Table 2 and Figure A6). The irregular shape of the RHA powder hampers a good powder packing in the microspheres, inhibiting grain diffusion during sintering. The total porosity of RHA-MS after sintering at 1400 °C is 67% as

determined by SEM analysis of the cross section. Sintering the FA-MS at 1400 °C resulted in a lower total porosity (50%). As indicated in the drying behaviour, more compact powder packing occurred in the FA-MS due to the broad size distribution of FA powder. This enhanced the densification of the FA-MS microspheres. In addition a unique microstructure could be observed on their cross section. The initial FA powder consists of a combination of dense and hollow spherical particles. The incorporation of these hollow cenospheres gives specials features, allowing shaping lightweight microspheres.

The porosity of AS-MS is significantly lower (4%) with only a few pores visible on the cross section. The dilatometry analysis revealed an enhanced densification for the AS-MS microspheres, in correlation to the lowest total porosity after sintering at 1600 °C. The densification and by consequence the residual porosity in the microspheres has an impact on the crushing strength of the microspheres. Due to the crystallization of tridymite in the RHA-MS, the densification was restrained and therefore low strengths and high porosity were determined. The higher strength of FA-MS could be correlated to two factors: the decreased total porosity and the presence of elongated mullite grains. The elongated grains are the most effective morphology to deflect the propagation cracks in the microspheres, by twisting the crack front in between the powder particles[48]. Highest crushing strength of 185 MPa was obtained for the AS-MS, despite the AGG of Al_2O_3 in the mullite and amorphous calcium aluminium silicate[49].

Current work stipulates the impact of the waste composition and morphology on the properties of the sintered microspheres. Consequently high porosity and low strengths were obtained for the siliceous waste resources. Despite the limited flexibility of shaping microspheres with high strength from these waste fines, it would be promising the exploit their opportunities. Previous work indicated the possibility of mixing fly ash or rice husk ash with alumina to obtain mullite[43][50]. Mullite is a good candidate for structural applications because of its good chemical stability and high strength. Therefore, further work has to be done on smart mixing the waste streams to enhance their mechanical properties.

4. Conclusion

The versatile use of droplet coagulation to recycle complex waste resources was illustrated by shaping fine-grained waste powders. Rice husk ash (RHA), fly ash (FA) and alum sludge (AS) were selected due to their distinct differences in waste origin (e.g. sludge versus high temperature), composition (e.g. Si/Al ratio) and morphology. The distinct differences enabled us to investigate the generic use and impact of different waste powders on the pre-processing, shaping and post processing into microspheres via droplet

coagulation. RHA and FA originated from a high temperature process, allowing impurities to be embedded in the powder structure and resulting in low levels of organic materials, posing no substantial impact on the suspension and coagulation process. Only in the thermal post-processing, influences of differences in both composition and morphology in combination with the introduced calcium were observed. The alum sludge (AS) is produced in the waste water treatment and required extra pre-processing steps due to the presence of organic additives and NOM (natural organic matter). Prior to suspension preparation, AS had to be dried, calcined and milled to obtain a fine-grained powder. In addition, some washing steps were essential to decrease the free calcium content from 124 mg/L to 12,9 mg/l in order to prevent premature coagulation of the sodium alginate, negatively affecting rheology. Once a fluid suspension was obtained of the different powders, shaping could be performed without any impact of the powder characteristics. The effect of shaping was specific for all three waste materials, in correlation to their chemical composition. Besides the presence of calcium introduced in the microspheres via the coagulation mechanism, an effect of the initial waste impurities on the microspheres properties could be distinguished. The porosity of the FA and RHA microspheres after sintering remained relatively high (50% for FA and 67% for RHA), in contrast to the densified AS microspheres (4%). The differences in microstructure caused low mechanical strength for the FA and RHA microspheres. Highest crushing strength were obtained for the AS microspheres (185 MPa).

Acknowledgements

This research is supported by the Agency for Innovation by Science and Technology in Flanders (IWT-131229), which granted J. Pype her PhD scholarship. The authors thank ‘De Watergroep’, Jef Bergmans and Ruben Snellings for supplying the alum sludge and fly ash. The authors gratefully acknowledge the technical support of the VITO personnel (Unit sustainable materials management), especially A. De Wilde (TGA-MS), M. Mertens (XRD), R. Kemps and D. Vanhoyweghen (SEM-EDX). In addition they thank the VITO technical staff of the MANT unit for the XRF, ICP-AES and Ion chromatography analysis.

References

[1] P.T. Jones, D. Geysen, Y. Tielemans, S. Van Passel, Y. Pontikes, B. Blanpain, M. Quaghebeur, N. Hoekstra, Enhanced Landfill Mining in view of multiple resource recovery: A critical review, J. Clean. Prod. 55 (2013) 45–55. doi:10.1016/j.jclepro.2012.05.021.

[2] J.M. Allwood, M.F. Ashby, T.G. Gutowski, E. Worrell, Material efficiency: A white paper, Resour. Conserv. Recycl. 55 (2011) 362–381. doi:10.1016/j.resconrec.2010.11.002.

[3] N. Soltani, A. Bahrami, M.I. Pech-Canul, L.A. Gonzalez, Review on the physicochemical treatments of rice husk for production of advanced materials, Chem. Eng. J. 264 (2015) 899–935. doi:10.1016/j.cej.2014.11.056.

[4] S. De Gisi, G. Lofrano, M. Grassi, M. Notarnicola, Characteristics and adsorption capacities of low-cost sorbents for wastewater treatment: A review, Sustain. Mater. Technol. 9 (2016) 10–40. doi:10.1016/j.susmat.2016.06.002.

[5] P.J. Borm, Toxicity and occupational health hazards of coal fly ash (CFA). A review of data and comparison to coal mine dust., Ann. Occup. Hyg. 41 (1997) 659–676. doi:10.1016/S0003-4878(97)00026-4.

[6] M. Ahmaruzzaman, A review on the utilization of fly ash, Prog. Energy Combust. Sci. 36 (2010) 327–363. doi:10.1016/j.pecs.2009.11.003.

[7] S. Chandrasekhar, K.G. Satyanarayana, P.N. Pramada, P. Raghavan, T.N. Gupta, Review Processing, properties and applications of reactive silica from rice husk—an overview, J. Mater. Sci. 38 (2003) 3159–3168. doi:10.1023/A:1025157114800.

[8] K.B. Dassanayake, G.Y. Jayasinghe, A. Surapaneni, C. Hetherington, A review on alum sludge reuse with special reference to agricultural applications and future challenges, Waste Manag. 38 (2015) 321–335. doi:10.1016/j.wasman.2014.11.025.

[9] R.S. Blissett, N.A. Rowson, A review of the multi-component utilisation of coal fly ash, Fuel. 97 (2012) 1–23.

[10] J.S. Lim, Z.A. Manan, S.R. Wan Alwi, H. Hashim, A review on utilisation of biomass from rice industry as a source of renewable energy, Renew. Sustain. Energy Rev. 16 (2012) 3084–3094. doi:10.1016/j.rser.2012.02.051.

[11] Y. Yang, Y.Q. Zhao, A.O. Babatunde, L. Wang, Y.X. Ren, Y. Han, Characteristics and mechanisms of phosphate adsorption on dewatered alum sludge, Sep. Purif. Technol. 51 (2006) 193–200. doi:10.1016/j.seppur.2006.01.013.

[12] R.C. Kaggwa, C.I. Mulalelo, P. Denny, T.O. Okurut, The impact of alum discharges on a natural tropical wetland in Uganda, Water Res. 35 (2001) 795–807.

doi:10.1016/S0043-1354(00)00301-8.

[13] Y. Jia, Y. Kanno, Z. peng Xie, New gel-casting process for alumina ceramics based on gelation of alginate, J. Eur. Ceram. Soc. 22 (2002) 1911–1916. doi:10.1016/S0955-2219(01)00513-1.

[14] M.I. Nieto, I. Santacruz, R. Moreno, Shaping of dense advanced ceramics and coatings by gelation of polysaccharides, Adv. Eng. Mater. 16 (2014) 637–654. doi:10.1002/adem.201400076.

[15] A.R. Studart, V.C. Pandolfelli, E. Tervoort, L.J. Gauckler, Gelling of Alumina Suspensions Using Alginic Acid Salt and hydroxylaluminium diacetate, J. Am. Ceram. Soc. 18 (2002) 2711–2718. doi:10.1111/j.1151-2916.2002.tb00518.x.

[16] J. Ma, Z. Xie, H. Miao, B. Zhang, X. Lin, Y. Cheng, Gelcasting of alumina ceramic components in nontoxic Na-alginate–CaIO3–PVP systems, Mater. Des. 26 (2005) 291–296. doi:10.1016/j.matdes.2004.06.011.

[17] C. Brandes, L. Treccani, S. Kroll, K. Rezwan, Gel casting of free-shapeable ceramic membranes with adjustable pore size for ultra- and microfiltration, J. Am. Ceram. Soc. 97 (2014) 1393–1401. doi:10.1111/jace.12877.

[18] J. Pype, B. Michielsen, E.M. Seftel, S. Mullens, V. Meynen, Development of alumina microspheres with controlled size and shape by vibrational droplet coagulation, J. Eur. Ceram. Soc. 37 (2017) 189–198. doi:10.1016/j.jeurceramsoc.2016.07.020.

[19] B.-B. Lee, P. Ravindra, E.-S. Chan, Size and Shape of Calcium Alginate Beads Produced by Extrusion Dripping, Chem. Eng. Technol. (2013) 1627–1642. doi:10.1002/ceat.201300230.

[20] E.-S. Chan, B.-B. Lee, P. Ravindra, D. Poncelet, Prediction models for shape and size of ca-alginate macrobeads produced through extrusion-dripping method., J. Colloid Interface Sci. 338 (2009) 63–72. doi:10.1016/j.jcis.2009.05.027.

[21] A. Licciulli, M. Notaro, S. De Santis, C. Terreni, S.K. Padmanabhan, CO2 capture on amine impregnated mesoporous alumina-silica mixed oxide spheres, Fuel Process. Technol. 166 (2017) 202–208. doi:https://doi.org/10.1016/j.fuproc.2017.06.009.

[22] J.M.F. Ferreira, S.M. Olhero, Al-rich sludge treatments towards recycling, J. Eur. Ceram. Soc. 22 (2002) 2243–2249. doi:10.1016/S0955-2219(02)00023-7.

[23] C.S. Lee, J. Robinson, M.F. Chong, A review on application of flocculants in wastewater treatment, Process Saf. Environ. Prot. 2 (2014) 489–508. doi:10.1016/j.psep.2014.04.010.

[24] C.J.E. Santos, T.-S. Wei, B. Cho, W.M. Kriven, A Forming Technique to Produce Spherical Ceramic Beads Using Sodium Alginate as a Precursor Binder Phase, J. Am. Ceram. Soc. 96 (2013) 3379–3388. doi:10.1111/jace.12584.

[25] C. Couroyer, M. Ghadiri, P. Laval, N. Brunard, F. Kolenda, Methodology for Investigating the Mechanical Strength of Reforming Catalyst Beads, Oil Gas Technol. 55 (2000) 67–85.

[26] G.C. Cordeiro, R.D. Toledo Filho, E. de Moraes Rego Fairbairn, Use of ultrafine rice husk ash with high-carbon content as pozzolan in high performance concrete, Mater. Struct. 42 (2009) 983–992. doi:10.1617/s11527-008-9437-z.

[27] S.D. Genieva, S.C. Turmanova, A.S. Dimitrova, L.T. Vlaev, Characterization of rice husks and the products of its thermal degradation in air or nitrogen atmosphere, J. Therm. Anal. Calorim. 93 (2008) 387–396. doi:10.1007/s10973-007-8429-5.

[28] J. Payá, J. Monzó, M.. Borrachero, E. Perris, F. Amahjour, Thermogravimetric Methods for Determining Carbon Content in Fly Ashes, Cem. Concr. Res. 28 (1998) 675–686. doi:10.1016/S0008-8846(98)00030-1.

[29] Y. Yang, Y.Q. Zhao, P. Kearney, Influence of ageing on the structure and phosphate adsorption capacity of dewatered alum sludge, Chem. Eng. J. 145 (2008) 276–284. doi:10.1016/j.cej.2008.04.026.

[30] Y. Pelovski, W. Pietkova, I. Gruncharov, B. Pacewska, J. Pysiak, The thermal decomposition of aluminum sulfate in different gas phase environments, Thermochim. Acta. 205 (1992) 219–224.

[31] T.Y. Klein, L. Treccani, K. Rezwan, Ceramic Microbeads as Adsorbents for Purification Technologies with high specific surface area, adjustable pore size and morphology obtained by ionotropic gelation, J. Am. Ceram. Soc. 95 (2012) 907–914.

[32] C.C. Ribeiro, C.C. Barrias, M.A. Barbosa, Preparation and characterisation of calcium-phosphate porous microspheres with a uniform size for biomedical applications, J. Mater. Sci. Mater. Med. 17 (2006) 455–463. doi:10.1007/s10856-006-8473-x.

[33] A. Haug, O. Smidsrød, B. Larsen, S. Gronowitz, R.A. Hoffman, A. Westerdahl, The Effect of Divalent Metals on the Properties of Alginate Solutions. II. Comparison of Different Metal Ions., Acta Chem. Scand. 19 (1965) 341–351. doi:10.3891/acta.chem.scand.19-0341.

[34] A. Haug, O. Smidsrod, The Effect of Divalent Metals on the Properties of Alginate Solutions. I. Calcium ions, Acta Chem. Scand. 19 (1965) 341–351. doi:10.3891/acta.chem.scand.19-0341.

[35] M.R. Davidson, J.J. Cooper-White, Pendant drop formation of shear-thinning and yield stress fluids, Appl. Math. Model. 30 (2006) 1392–1405. doi:10.1016/j.apm.2006.03.016.

[36] M.J. Ribeiro, D.U. Tulyaganov, J.M. Ferreira, J.A. Labrincha, Recycling of Al-rich

industrial sludge in refractory ceramic pressed bodies, Ceram. Int. 28 (2002) 319–326. doi:10.1016/S0272-8842(01)00097-9.

[37] E.S. Newman, Behavior of calcium sulfate at high temperatures, J. Res. Natl. Bur. Stand. (1934). 27 (1941) 191. doi:10.6028/jres.027.009.

[38] F. Peng, P. Di, Effect of multivalent Salts - Calcium and Aluminum on the flocculation of Kaolin Suspension with anionic polyacrylamide, J. Colloid Interface Sci. 164 (1994) 223–237.

[39] M.B. Mohd Salahuddin, M. Norkhairunnisa, F. Mustapha, A review on thermophysical evaluation of alkali-activated geopolymers, Ceram. Int. 41 (2015) 4273–4281. doi:10.1016/j.ceramint.2014.11.119.

[40] M.M. Haslinawati, K.A. Matori, Z.A. Wahab, H.A.A. Sidek, A.T. Zainal, Effect of Temperature on Ceramic from Rice Husk Ash, Int. J. Basic Appl. Sci. (2009) 1985–1988.

[41] J.R. Taylor, A.T. Dinsdale, Thermodynamic and phase diagram data for the CaO-SiO2 system, Calphad. 14 (1990) 71–88. doi:10.1016/0364-5916(90)90041-W.

[42] Y. Dong, X. Feng, X. Feng, Y. Ding, X. Liu, G. Meng, Preparation of low-cost mullite ceramics from natural bauxite and industrial waste fly ash, J. Alloys Compd. 460 (2008) 599–606. doi:10.1016/j.jallcom.2007.06.023.

[43] J.S. Jung, H.C. Park, R. Stevens, Mullite ceramics derived from coal fly ash, J. Mater. Sci. Lett. 20 (2001) 1089–1091. doi:10.1023/A:1010934728570.

[44] M.Y.A. Mollah, S. Promreuk, R. Schennach, D.L. Cocke, R. G??ler, Cristobalite formation from thermal treatment of Texas lignite fly ash, Fuel. 78 (1999) 1277–1282. doi:10.1016/S0016-2361(99)00057-5.

[45] S.C. Vieira, A.S. Ramos, M.T. Vieira, Mullitization kinetics from silica- and alumina-rich wastes, Ceram. Int. 33 (2007) 59–66. doi:10.1016/j.ceramint.2005.07.015.

[46] O.B. Fabrichnaya, I. Nerad, Thermodynamic properties of liquid phase in the CaO·SiO2–CaO·Al2O3·2SiO2–2CaO·Al2O3·SiO2 system, J. Eur. Ceram. Soc. 20 (2000) 505–515.

[47] C.W. Park, D.Y. Yoon, Abnormal Grain Growth in Alumina with Anorthite Liquid and the Effect of MgO Addition, J. Am. Ceram. Soc. 85 (2002) 1585–1593. doi:10.1111/j.1151-2916.2002.tb00316.x.

[48] K.T. Faber, A.G. Evans, Crack deflection processes-I. Theory, Acta Metall. 31 (1983) 565–576. doi:10.1016/0001-6160(83)90046-9.

[49] C. Brandes, M. Hoog Antink, S. Kroll, L. Treccani, K. Rezwan, Aluminium acetate as alternative cross-linker for temperature controlled gel-casting and joining of ceramics, J. Eur. Ceram. Soc. 36 (2016) 1241–1251.

doi:10.1016/j.jeurceramsoc.2015.12.011.

[50] M.F. Serra, M.S. Conconi, M.R. Gauna, G. Suárez, E.F. Aglietti, N.M. Rendtorff, Mullite (3Al2O3·2SiO2) ceramics obtained by reaction sintering of rice husk ash and alumina, phase evolution, sintering and microstructure, J. Asian Ceram. Soc. 4 (2015) 1–7. doi:10.1016/j.jascer.2015.11.003.